Clim. Past Discuss., 7, 347–379, 2011
www.clim-past-discuss.net/7/347/2011/
doi:10.5194/cpd-7-347-2011

Climate of the Past Discussions

Interhemispheric gradient of atmospheric radiocarbon reveals natural variability of Southern Ocean winds

K. B. Rodgers[1], S. E. M. Fletcher[1,2], D. Bianchi[1], C. Beaulieu[1], E. D. Galbraith[1], A. Gnanadesikan[3], A. G. Hogg[4], D. Iudicone[5], B. Lintner[6], T. Naegler[7,8], P. J. Reimer[9], J. L. Sarmiento[1], and R. D. Slater[1]

[1]AOS Program, Princeton University, Princeton, NJ, USA
[2]National Institute for Water and Atmospheric Research, Wellington, New Zealand
[3]Geophysical Fluid Dynamics Laboratory, Princeton, NJ, USA
[4]Carbon Dating Laboratory, University of Waikito, Hamilton, New Zealand
[5]Stazione Zoologica Anton Dohrn, Naples, Italy
[6]Rutgers University, New Brunswick, NJ, USA
[7]Institute for Environmental Physics, University of Heidelberg, Germany
[8]German Aerospace Center, Institute for Technical Thermodynamics, Department of System Analysis and Technology Assessment, Stuttgart, Germany
[9]Queens University, Belfast, UK

Received: 14 January 2011 – Accepted: 17 January 2011 – Published: 25 January 2011

Correspondence to: K. B. Rodgers (krodgers@princeton.edu)

Published by Copernicus Publications on behalf of the European Geosciences Union.

Abstract

Tree ring $\Delta^{14}C$ data (Reimer et al., 2004; McCormac et al., 2004) indicate that atmospheric $\Delta^{14}C$ varied on multi-decadal to centennial timescales, in both hemispheres, over the pre-industrial period AD 950–1830. Although the Northern and Southern Hemispheric $\Delta^{14}C$ records display similar variability, it is difficult from these data alone to distinguish between variations driven by $^{14}CO_2$ production in the upper atmosphere (Stuiver, 1980) and exchanges between carbon reservoirs (Siegenthaler, 1980). Here we consider rather the Interhemispheric Gradient in atmospheric $\Delta^{14}C$ as revealing of the background pre-bomb air-sea Disequilbrium Flux between $^{14}CO_2$ and CO_2. As the global maximum of the Disequilibrium Flux is squarely centered in the open ocean regions of the Southern Ocean, relatively modest perturbations to the winds over this region drive significant perturbations to the Interhemispheric Gradient. The analysis presented here implies that changes to Southern Ocean windspeeds are likely a main driver of the observed variability in the Interhemispheric Gradient over 950–1830, and further, that this variability may be larger than the Southern Ocean wind trends that have been reported for recent decades (notably 1980–2004). This interpretation also implies a significant weakening of the winds over the Southern Ocean within a few decades of AD 1375, associated with the transition between the Medieval Climate Anomaly and the Little Ice Age. The driving forces that could have produced such a shift in the winds remain unkown.

1 Introduction

The tree ring $\Delta^{14}C$ data from INTCAL04 (Reimer et al., 2004) and SHCAL04 (McCormac et al., 2004) indicate that over the period 950–1830, atmospheric $\Delta^{14}C$ varied on multi-decadal to centennial timescales in both hemispheres (the temporal resolution of each record is five years) (Fig. 1a). The earlier part of the record is characterized by an atmosphere that is more depleted in $^{14}CO_2$ (e.g. relatively negative per mil values),

followed by a change towards an atmosphere more enriched in $^{14}CO_2$ (e.g. relatively positive per mil values) during the 14th century. Although the Northern and Southern Hemispheric records taken together provide evidence of synchronous variations over nearly all timescales, it is difficult from these data alone to identify the degree to which the variations in $\Delta^{14}C$ are driven by changes in the production of $^{14}CO_2$ in the upper atmosphere, and the degree to which they are driven by variations in the physical state of the system and the ensuing perturbations to the partitioning of $^{14}CO_2$ and CO_2 (and $^{13}CO_2$) between the oceanic, atmospheric, and terrestrial carbon reservoirs.

We calculate the difference between the two high-resolution tree-ring-derived hemispheric $\Delta^{14}C$ reconstructions, shown in Fig. 1a, to arrive at a timeseries for the Interhemispheric Gradient, shown in Fig. 1b. Given that about half of the ^{14}C production occurs in the stratosphere (Masarik and Beer, 1999), it is conceivable that different (and time-varying) stratosphere-troposphere exchange between the two hemispheres could contribute to changes in the Interhemispheric Gradient in the absence of changes in surface fluxes. However, the modeling study of Levin et al. (2009) revealed that this effect is small, and thus we assume here that changes in the stratospheric source of $^{14}CO_2$ do not project into large gradients in $\Delta^{14}C$ in the atmospheric boundary layer. It follows from this assumption that changes in the Interhemispheric Gradient are controlled by surface fluxes.

The Interhemispheric Gradient has persistent negative values, reflecting the fact that the Southern Hemisphere $\Delta^{14}C$ tends to be lower than it is in the Northern Hemisphere (Fig. 1b). Analysis reveals that this time series contains red noise, with variability in evidence on all timescales. Turney and Palmer (2007) previously considered the general structure of the Interhemispheric Gradient changes shown in Fig. 1b and argued that there was a significant change associated with the transition between the Medieval Climate Anomaly and the Little Ice Age during the 14th century, which they attributed to changes in ENSO. We conducted a change point analysis test of the timeseries following Worsley (1979), which identified a statistically significant (>99% confidence level) shift in 1375 in agreement with Turney and Palmer (2007). This point marks a

change between a mean Interhemispheric Gradient of −6.63‰ for the earlier part of the record and −4.48‰ for the later part of the record, implying a change in surface fluxes of radiocarbon.

Our goal in this study is to use models to test the hypothesis that changes of the Interhemispheric Gradient, such as the change identified at 1375, are most likely to reflect past changes of the integrated strength of the winds over the Southern Ocean. The recent study of Skinner et al. (2010) provided evidence that the Southern Ocean may be a critical player in determining the atmospheric $\Delta^{14}C$ response to an even larger perturbation earlier in the deglaciation. In contrast, earlier modeling studies that focused on variations in the Meridional Overturning Circulation of the North Atlantic as a potential driver of the large Younger Dryas transient in atmospheric $\Delta^{14}C$ were not able to fully explain the observed atmospheric $\Delta^{14}C$ during this period, even with a complete shutdown of the Meridional Overturning Circulation (Marchal et al., 2001; Meissner, 2007).

2 Model configuration

To facilitate our focus on understanding the processes that drive interhemispheric gradients in $\Delta^{14}C$, we have chosen to use a modeling configuration that consists of an ocean model and an Atmospheric Transport Model that are run sequentially rather than coupled. This enables us to control the Southern Ocean winds independently. The ocean model is first run to steady state for its ocean interior $\Delta^{14}C$ distribution. Both DIC and $DI^{14}C$ concentrations are set initially to 2000 µmol/kg. For DIC, convergence with the spinup is tested by the constraint that globally integrated air-sea CO_2 fluxes must be less than 0.01 Pg C/yr. For $\Delta^{14}C$, the convergence test is that 98% of the ocean interior volume should have drift of less than 0.001 per year (Aumont, 1998). This is then followed by the idealized ocean perturbation studies, with the perturbation consisting of scalar multiplication of the strength of the winds over the Southern Ocean.

The Atmospheric Transport Model is run using output from the ocean model perturbation experiments as its lower boundary conditions. The tracers $^{14}CO_2$ and CO_2 are advected and mixed in a global atmospheric model, and the sources and sinks are described below. In the perturbation studies here, there is an inherent inconsistency in that the wind stress perturbations used with the ocean model are not contained in the atmospheric circulation fields used for the transport model, since each perturbation experiment uses identical atmospheric circulation and mixing. We will later demonstrate that the Interhemispheric Gradient in $\Delta^{14}C$ is relatively insensitive to the interhemispheric exchange time.

2.1 Ocean model

The ocean code used here is Version 3 of the GFDL Modular Ocean Model (MOM3) (Pacanowski and Griffies, 1999). The model, which has 4° horizontal resolution and 24 vertical levels, is forced at the surface with buoyancy fluxes from the climatology of DaSilva et al. (2004), corrected as described in Gnanadesikan et al. (2004). Temperature is restored to observations with a timescale of 30 days over the 25m-thick surface layer while salinity is restored to surface values with a 120 day time scale at all points except for four coastal points around the Antarctic where subsurface salinity values and a 30 day restoring are used to ensure formation of the proper watermasses during the winter. Wind stress is taken with the ECMWF climatology (Trenberth et al., 1989). The control model corresponds to the P2A model of Gnanadesikan et al. (2004).

The representation of $\Delta^{14}C$ in the model follows the OCMIP-2 protocol (http://www.ipsl.jussieu.fr/OCMIP/phase2/), using the gas exchange parameterization of Wanninkhof (1992). The atmospheric $\Delta^{14}C$ is maintained at 0 for all experiments presented here, and the atmospheric CO_2 concentration is maintained at 278 µatm. A caveat with the OCMIP-2 representation of $\Delta^{14}C$ is that ^{13}C is ignored, despite the fact that it can play a non-negligible role in determining $\Delta^{14}C$ (see Appendix 1 for a more detailed description of $\Delta^{14}C$ as a tracer).

Surface wind stresses τ are calculated using a quadratic bulk formula:

$$\tau \rho C_d \boldsymbol{u}|\boldsymbol{u}|$$

where ρ is the density of air, C_d is a dimensionless drag coefficient, and $\boldsymbol{u}$ is the horizontal surface wind vector at 10 m. Likewise gas exchange is calculated using the formula from Wanninkhof (1992):

$$k_{\mathrm{av}} = 0.337|\boldsymbol{u}_{av}|^2(Sc/660)^{0.5}$$

where k_{av} is the piston velocity, Sc is the Schmidt number, etc., and $\boldsymbol{u}$ is the horizontal surface wind vector at 10 m. In fact Wanninkhof (1992) had specified 0.39 for the coefficient on the right hand side, and 0.337 is the coefficient for the right hand side chosen for the OCMIP-2 protocol. It is known that the Wanninkhof (1992) parameterization suffers from a number of limitations that have been described in Krakauer et al. (2006), Naegler et al. (2006), Sweeney et al. (2007), and Naegler (2009). These studies have demonstrated that the value resulting from the Wanninkhof (1992) parameterization is too large. For the calculations performed here, we have chosen to use the quadratic Wanninkhof (1992) parameterization in order to be consistent with previous studies with the same ocean model (Gnanadesikan et al., 2002; Gnanadesikan et al., 2004). However, a new study currently underway is investigating the sensitivity of the disequilibrium flux to the choice of gas exchange parameterization (Joe Majkut, personal communication, 2011).

2.2 Atmospheric transport model

The Atmospheric Transport Model Tracer Model 3 Version 3 (Heimann and Körner, 2003) was used for this study. This is a three-dimensional Eulerian model driven by offline wind fields. Here we have used both a coarse grid resolution (7.8° latitude by 10° longitude with nine vertical levels) and a fine grid resolution (4.4° latitude by 5° longitude with 19 vertical levels) version of the model in order to get a lower level estimate of the uncertainty associated with errors in the Atmospheric Transport Model

following Rödenbeck et al. (2008). The fine grid resolution has been shown to be substantially less diffusive in simulations of point sources, radon, and SF_6 (Heimann and Körner, 2003).

The wind fields used for the experiments here were taken from the NCEP reanalysis (Kalnay et al., 1996). Six different simulations were run with the Atmospheric Transport Model using repeating wind fields from 1995 to 2000, with the six different 20 year simulations performed by looping repeatedly over one of each of the 6 years spanning 1995 and 2005. The resulting tracer distributions from the five model runs were averaged to create a climatological field. Five different flux processes were prescribed in the model: air-sea fluxes of CO_2, air-sea fluxes of $^{14}CO_2$, stratospheric production of ^{14}C, terrestrial disequilibrium of ^{14}C, and a neutral terrestrial biosphere for CO_2. Each was treated as a separate tracer, and all five are combined to calculate atmospheric gradients of $\Delta^{14}C$. Air-sea fluxes of CO_2 and $^{14}CO_2$ are taken directly from the ocean model output. In addition, we included a source in the mid-to-upper stratosphere due to production by cosmogenic radiation, adapted from the source function of Turnbull et al. (2009). The magnitude of the atmospheric source was tuned such that it was consistent with air-sea fluxes of $^{14}CO_2$ from the ocean model.

Finally, we included a modest disequilibrium sink due to the residence time of carbon in the terrestrial biosphere. While the terrestrial biosphere is known to have a substantial disequilibrium in modern times due to the transient effect of bomb-generated $^{14}CO_2$, for the pre-anthropogenic period the pre-industrial disequilbrium is thought to have been small, as the residence time of CO_2 in the terrestrial biosphere is short relative to its radioactive decay timescale (Siegenthaler, 1986). A simple estimate based on the lifetime of ^{14}C in the biosphere and the mass of the biosphere suggests that the pre-anthropogenic terrestrial disequilibrium must be no more than 7% of the oceanic disequilibrium. We therefore formulated a simple representation of the biospheric disequilibrium flux by calculating the global total disequilibrium as 7% of the ocean value and distributed it spatially according to the absolute value of the Carnegie Ames Stanford Approach (CASA) neutral biosphere (Randerson et al., 1997). In addition, the CASA

neutral biosphere was used to simulate seasonal rectification in CO_2 and $^{14}CO_2$, although this effect is relatively negligible for $\Delta^{14}C$. The radioactive decay of ^{14}C in the atmosphere was neglected because the decay-time of ^{14}C is very long relative to the duration of the simulations.

The Atmospheric Transport Model is used together with the OGCM to explore the sensitivity of the Interhemispheric Gradient to idealized wind perturbations over the Southern Ocean. This sensitivity was evaluated by first perturbing the P2A configuration of the ocean model through a scalar multiplication of the wind stress (used for dynamics) and wind speed (used for tracer gas exchange) over the entire region south of 30° S. This test was motivated by the fact that surface atmospheric wind perturbations can impact oceanic $\Delta^{14}C$ both through changes to the physical state of the ocean in the absence of changes in gas exchange, as well as changes in gas exchange in the absence of perturbations to the circulation state. Of course the two types of perturbations in general will not be completely independent, but nevertheless this sensitivity is important to test for a mechanistic interpretation. Thus this idealized perturbation is analogous to that used with the same ocean model in the previous study of Mignone et al. (2006) (although in the study of Mignone et al. (2006) the perturbation was applied only to the dynamical perturbation but not in the gas exchange formulation). The perturbation here is applied to the amplitude but not the structure of the winds over the Southern Ocean. The idealized perturbations with the ocean model were applied over a period of 20 years, and the monthly air-sea fluxes of CO_2 and $^{14}CO_2$ from the ocean model over years 11–20 were used as the lower boundary condition for the Atmospheric Transport Model experiments. This is done for 10 separate cases, for perturbations spanning wind multiplicative factors of 0.6 to 1.5 in intervals of 0.1.

3 Results

We begin by looking at the annual mean air-sea flux for CO_2 (Fig. 2a) and $^{14}CO_2$ (Fig. 2b) for the model. The air-sea flux of $^{14}CO_2$ has been scaled by a multiplicative factor (0.85×10^{12}) as a means of normalizing the flux to the pre-anthropogenic late 19th century atmospheric value of $\Delta^{14}C = 0‰$. This scaling allows us to define the Disequilibrium Flux ϕ_{diseq}:

$$\phi_{\text{diseq}} = \phi_{14C} r^{12/14} - \phi_{12C}$$

where ϕ_{14C} is the air-sea flux of $^{14}CO_2$, $r^{12/14}$ is the pre-bomb atmospheric $^{12}C/^{14}C$ ratio, and ϕ_{12C} is the air-sea flux of CO_2. The annual mean distribution of this field is shown in Fig. 2c. Negative (blue) values indicate a tendency for the flux of $^{14}CO_2$ into the ocean to be larger than the flux of CO_2, thereby driving the atmospheric $\Delta^{14}C$ towards negative values from the pre-anthropogenic steady state of $\Delta^{14}C = 0$. The model has globally negative global mean ϕ_{diseq} values due to the fact that ^{14}C is produced by spallation in the upper atmosphere, and transferred across the air-sea boundary to balance the decay of $DI^{14}C$ in the ocean interior. (As noted above, this study will also account for the 7% contribution of the terrestrial biosphere to the global ϕ_{diseq}). The zonal integral of ϕ_{diseq} is shown in Fig. 2d. The total ϕ_{diseq} into the ocean is 3.6 GtC/yr, with 74% occurring in the Southern Hemisphere and 62% south of 30° S. A 1.8 GtC/yr difference in the disequilibrium flux between the Northern and Southern Hemispheres would be expected to produce an interhemispheric flux of 0.9 GtC/yr within the atmosphere as the atmosphere came into equilibrium. Given an interhemispheric exchange time of order 1.3 yr (Geller et al., 1997) this would imply a 1.17 GtC equivalent interhemispheric difference in the atmospheric radiocarbon inventory. Given a preindustrial tropospheric carbon inventory of ∼480 Gt C – or 240 Gt C/hemisphere, this would correspond to a difference of 4.9‰. This value is within 20% of the mean Interhemispheric Gradient seen in Fig. 1b. This mass balance calculation illustrates how the ϕ_{diseq} at the sea surface is the fundamental driver of the Interhemispheric Gradient.

This simple scaling argument is more rigorously confirmed using the Atmospheric Transport Model. For the P2A simulation performed with the MOM3 model, a corresponding simulation was performed with the Atmospheric Transport Model using the air-sea fluxes of CO_2 from the ocean model over a period of 10 years (the Interhemispheric Gradient converges in less than two years). Although the amplitude of the Interhemispheric Gradient converges quickly, we are specifically interested in the multi-decadal (and longer) timescale variations revealed in Fig. 1b. Therefore, we also consider other sources and sinks of $^{14}CO_2$ in the Earth system, including the production of $^{14}CO_2$ in the upper atmosphere and fluxes between the atmosphere and the terrestrial biosphere. The mean meridional structure of $\Delta^{14}C$ in the atmospheric boundary layer is shown in Fig. 3 (black curve). The $\Delta^{14}C$ activity is shown as a deviation from the value at the North Pole in order to emphasize the amplitude and structure of the meridional gradient. Additionally the large-scale meridional structure is controlled by the ocean fluxes. The resulting model shows a difference of about 3 between the mid-latitude Northern and Southern Hemispheres. This is smaller than the observed gradient, and is also smaller than the gradient estimated from the simple scaling arguments. This suggests that the transport model may be overestimating interhemispheric exchange.

The tendency for a global maximum in the absolute value of ϕ_{diseq} over the Southern Ocean is the result of two factors. The first is that the Southern Ocean is where the most depleted waters come to the surface, as illustrated in Fig. 4a using the pre-bomb data product for $\Delta^{14}C$ from GLODAP (Key et al., 2004) along a continuous track running from the North Atlantic to the Southern Ocean to the North Pacific. Surface waters in the Southern Ocean are poorly equilibrated, with values of −120‰, while North Atlantic waters are closer to −50‰, and thereby the average flux to the ocean is twice as large per unit area over the Southern Ocean. Our model (Fig. 4b) captures this pattern of $\Delta^{14}C$ activities relatively well. Additionally, the larger areal extent of the Southern ocean means that this larger flux (per unit area) produces a significantly larger integrated uptake of $^{14}CO_2$ than the North Atlantic.

Next we consider the disribution of $\Delta^{14}C$ in the atmospheric Transport Model, with the fluxes from the perurbation experiments from the ocean model used as a lower boundary. The Interhemispheric Gradient (the deviation of the zonal mean surface atmospheric activities from the $\Delta^{14}C$ activity at the North Pole) is shown in Fig. 5a for the case where the scalar perturbation to the winds has been applied to both the wind stress (used for dynamical forcing) and the surface wind speed (used for gas exchange). The figure reveals a clear response in the Interhemispheric Gradient to the strength of the winds over the Southern Ocean, with a larger Interhemispheric Gradient corresponding to stronger winds. Whereas the Interhemispheric Gradient is nearly 3‰ at 55° S for the control case (p2a_1.0), it is in excess of 6.0‰ for the p2a_1.4 case, and of order 2.0‰ for the p2a_0.5 case. For the p2a_1.0 case, we note here that the mean gradient as simulated is smaller (by 35%) than what is found in the data for the mean (Fig. 1b) as well as according to the scaling argument presented in Sect. 2. A number of factors are expected contribute to the under-estimation of the Interhemispheric Gradient in the model simulation, including numerical biases and biases in the atmospheric transport fields. For this reason the disagreement between the mean Interhemispheric Gradient between Fig. 1b (Data proxy) and Fig. 4a (p2a_1.0 simulation) is within the range of uncertainty with such models.

In order to evaluate whether the Interhemispheric Gradient shown in Fig. 5a is controlled primarily by the wind stress (which directly impacts the ocean circulation through the momentum equations) or the wind speed (which only acts on tracers through the gas exchange parameterization), we conducted two additional sets of perturbation studies with the ocean model (Fig. 5b,c). The information shown in Fig. 5a–c is reconsidered in a scatterplot in Fig. 6 for the case of the difference in the mean $\Delta^{14}C$ north of 30° S and the mean $\Delta^{14}C$ south of 30° S. The green triangles represent the full signal, the red squares represent the sensitivity to windspeed perturbations, and blue diamonds represent the sensitivity to windstress perturbations. For the full signal, the analysis reveals that perturbations of slightly larger than 20% in the windspeed are able to account for 1.6‰ changes in the Interhemispheric Gradient over an interval

of two decades. The dependence of gas exchange rates on windspeed dominates over the effect of wind stress on ocean circulation. When both effects are included, perturbations of slightly larger than 20% in the windspeed produce changes in the Interhemispheric Gradient of order 1.6 over the interval of two decades. Given our prior assumptions, this suggests that natural variability of Southern Ocean winds over the past millenium have been of order 20%.

To put such variability in context, we compare it to the trend in Southern Ocean winds that is widely interpreted as being an anthropogenic perturbation over 1980–2004 (the period of focus of the study of Le Quéré et al., 2007). Here we focus on the surface winds in the NCEP-1 reanalysis (Kalnay et al., 1996) that served as the forcing for the ocean modeling component of the study of Le Quéré et al. (2007). The time-mean 10 meter windspeeds over 1949–2008 are shown in Fig. 7a, and the monthly average of the windspeeds over the latitude band 40° S–60° S are shown in Fig. 7b. Over the period 1980–2004, a linear trend analysis indicates a rate of increase in wind strength corresponding to a 10% increase over that interval. This observed change over 2–1/2 decades is in fact less than what were infere here to be the natural background variability of the surface wind strength over decadal timescales over the Southern Ocean from Fig. 6. There is a wide consensus that a significant part of the trend over 1980–2004 can be attributed to the effects of ozone and climate. What we wish to emphasize here is that the natural variability over the pre-anthropogenic period may have been at least as large as the anthropogenic trend detected over recent decades.

4 Discussion

This study suggests that the trend towards increased windspeeds over the Southern Ocean over recent decades may be of the same amplitude as the natural background variability over decadal timescales for the interval AD 950–1830. This new result could not have been inferred from proxies of wind variability that span the period of the instrumental record (AD 1884-present) (Visbeck, 2009) as instrument-based records are

also too short to characterize the spectral characteristics of decadal-to-multi-decadal background variations in the conditions over the Southern Ocean.

Our results also imply that a weakening of the winds over the Southern Ocean could have been associated with the transition between the Medieval Climate Anomaly and the Little Ice Age. Change point analysis of tree ring $\Delta^{14}C$ reveals that the Interhemispheric Gradient decreased by 2.2‰ about AD 1375, and this is consistent with a weakening of the winds over the Southern Ocean. One should certainly exercise caution in using the results of the 20-year sensitivity calculation in Fig. 6 to infer the magnitude of the centennial timescale changes evident in Fig. 1b about AD 1375. It is worth noting that changes in large-scale interhemispheric exchange time could also play a role in altering Interhemispheric Gradient. However, a scaling argument for the impact of the interhemispheric exchange rate on the interhemispheric gradient supports our main contention that the Southern Ocean winds control the multi-decadal and longer timescale changes in the Interhemispheric Gradient shown in Fig. 1b. For modern conditions, the difference in the interhemispheric exchange timescale for tracers between extreme El Niño and La Niña years is 0.05–0.10 years, according to the study of Lintner et al. (2004) using the NCEP MATCH (Model of Atmospheric Transport and Chemistry) model. Relative to this model's mean exchange time (0.86 years, based on averages over the whole vertical column as opposed to surface concentrations as in Geller et al., 1997), this constitutes a range in net interhemispheric exchange of order 6–12%. For comparable differences between the Medieval Climate Anomaly and the Little Ice Age, this would correspond to gradient differences of 0.3–0.6‰, which is significantly less than the observed difference of 2.2‰ between the Medieval Climate Anomaly and the Little Ice Age. Changes in the interhemispheric exchange rate 4–8 times the size of those associated with ENSO would thus be required to explain this signal. A much more detailed and process-focused modeling study of this is currently underway, and will be the subject of a future publication.

The inferred reduction in winds over the Southern Ocean may have been connected with many previously reported global scale changes. It is thought that the equatorial

Pacific exhibited a shift towards warmer conditions during the transition from the Medieval Climate Anomaly to the Little Ice Age (Cobb et al., 2003; Sachs et al., 2009). This would imply that a shift towards weakened winds over the Southern Ocean was contemporaneous with a shift towards warm conditions with more frequent ENSOs for the Equatorial Pacific. Weakening of winds over the Southern Ocean during the Medieval Climate Anomaly to Little Ice Age transition is a new result that has not been previously presented in the climate literature. Such a change hints at a potentially causative impact on the strength of the Atlantic Meridional Overturning circulation, given that Southern winds help to drive the Atlantic Meridional Overturning Circulation (Toggweiler and Samuels, 1993). We speculate that a weakening of the Southern Westerlies at AD 1375 would have contributed to a weakening of the Atlantic Meridional overturning, supported by proxy data (Lund et al., 2006), potentially reducing the heat transport into the northern North Atlantic and helping to usher in the Little Ice Age in the Northern Hemisphere.

A role for the Southern Ocean in sustaining the mean interhemispheric gradient in atmospheric $\Delta^{14}C$ was suggested in the earlier works of Braziunas et al. (1995), McCormac et al. (2002) and Levin and Hesshaimer (2000). All of these studies invoked mean conditions over the Southern Ocean to account for the mean interhemispheric gradient in atmospheric $\Delta^{14}C$. The current study differs from these earlier studies in two ways. First, our study has been the first to provide an account of Southern Ocean mechanisms that can sustain the mean Interhemispheric Gradient in $\Delta^{14}C$, as well as the time variability of this gradient. We have emphasized the value of the Disequilbrium Flux ϕ_{diseq} in understanding the Interhemispheric Gradient in $\Delta^{14}C$, and shown how it is connected to the large-scale overturning circulation of the ocean (Fig. 4). Second, whereas the focus of previous studies has been on the carbon cycle, we have chosen here to emphasize atmospheric $\Delta^{14}C$ as a dynamical tracer rather than as a tracer of the global carbon cycle. There may well be important implications of this dynamical interpretation (the Interhemispheric Gradient as a proxy for Southern Ocean wind variations) for the carbon cycle, but we have left this as a subject for future investigation.

A comparison of Figs. 1b and 5a revealed that there is a discrepancy between the simulated interhemispheric gradient in $\Delta^{14}C$. The fact that the simulated gradient is weaker than the gradient in the proxy record could derive from a number of sources. These include biases in: (1) the atmospheric state, (2) gas exchange, and (3) the oceanic state. For the atmospheric state, this could include biases in parameterizations of vertical transport and convection, the coarse resolution of the model, and biases in the climate state of the 1990s relative to the pre-anthropogenic period.

An additional source of uncertainty in the atmosphere could result from a rectifying effect involving the stratospheric/tropospheric exchange in the two hemispheres. The previous study of Randerson et al. (2002) considered the seasonal cycle of this exchange for $^{14}CO_2$ in both hemispheres (their Fig. 3), and pointed out that the seasonality is significantly larger in the North. The maximum injection of $^{14}CO_2$ occurs in the Northern Spring, corresponding to the season or springtime tree growth. A simple scaling can provide an estimate of the impact on the mean interhemispheric gradient. Assuming that the amplitude of the flux variability is $0.9\,\text{Gt C yr}^{-1}$ in scaled $^{14}CO_2$ units, the amplitude of the inventory variability is $0.9\,\text{Gt C}/(2\,\Pi) = 0.14\,\text{Gt C} = 0.58‰$. Including this rectifying effect would then increase the Interhemispheric Gradient by nearly 20%.

Another potential source of uncertainty could be the parameterization of mesoscale eddies in the Southern Ocean. A number of studies (notably those of Straub, 1993; Hallberg and Gnanadesikan, 2006; Böning et al., 2009; and Farneti et al., 2010) have argued that the type of non-eddying ocean model used here may exaggerate the dynamical response of the Southern Ocean to wind perturbations. However, the dominance of wind speed (which drives changes in gas exchange) over the influence of wind stress (which drives changes in upwelling) suggests that the variations in the Interhemispheric Gradient of $\Delta^{14}C$ in Fig. 1b is robust no matter what the eventual resolution of the role of ocean eddies may be. Given the strength of the winds over the Southern Ocean, this case would be stronger yet if a cubic wind speed-dependence for gas exchange (Wanninkhof and McGillis, 1999) turns out to be more appropriate

than the quadriatic formulation used here. Additionally, it is important to emphasize that the model configuration presented here has been used to test the sensitivity to the strength of the Southern Ocean winds, but not the latitude of the position of the maximum westerlies over the Southern Ocean. The type of perturbation chosen here finds justification in the results of d'Orgeville et al. (2010) who demonstrated for the case of CO_2 that the sensitivity to wind strength is significantly stronger than the sensitivity to the longitude of the maximum westerlies. The sensitivity to latitude for the case of $\Delta^{14}C$ along with CO_2 is left as a subject for future investigation.

Recent analysis of a coupled ocean-atmosphere model with steady solar and radiative forcing that includes $\Delta^{14}C$ as a tracer (Galbraith et al., 2011) is consistent with variability in the Southern Hemisphere dominating air-sea exchange of $^{14}CO_2$. However, the unforced decadal-to-multidecadal variability of Southern Ocean winds exhibited by this coupled model is of much smaller magnitude than inferred from the analysis here. This would seem to suggest that an external driver, such as solar, volcanic or ice sheet variability, could be inferred to drive changes in the Southern Westerlies, as part of the climate's trajectory toward the Little Ice Age.

This paper has argued for a relatively simple link between the Interhemispheric Gradient and surface ocean fluxes, dominated by wind-driven changes over the Southern Ocean primarily through their impact on gas exchange. As such, the Interhemispheric Gradient in atmospheric $\Delta^{14}C$ could serve as a powerful new proxy integrating the Southern westerly wind strength over large temporal and spatial scales. We note that the $\Delta^{14}C$ gradient within the Southern Hemisphere is also significant (black line in Fig. 3) in addtion to the overall Interhemispheric Gradient in $\Delta^{14}C$. Thus documenting more precisely latitudinally-resolved $\Delta^{14}C$ records may help to better constrain past changes in the Diseqiulibrium Flux ϕ_{diseq}. It is our intention that future work will incorporate $\Delta^{14}C$ as a fully prognostic atmospheric as well as oceanic tracer in ensemble calculations with a coupled model (following the work of Jungclaus et al., 2010).

Appendix A

$\Delta^{14}C$ as a tracer

Radiocarbon (^{14}C) is the radioactive isotope of carbon with a half-life of 5730 years. Radiocarbon activities are usually reported as $\Delta^{14}C$. For practical purposes this is the deviation in per mil units (parts per thousand) of the ratio $^{14}C/^{12}C$ from a decay-corrected isotopic standard (Stuiver and Polach, 1977), including a ^{13}C-normalization for isotopic fractionation where, as an approximation, it has often been assumed that the fractionation is twice as large for ^{14}C as for ^{13}C. A precise definition of $\Delta^{14}C$ has been presented in the study of Stuiver and Polach (1977):

$$\Delta^{14}C = 1000. \cdot \{[(1 + (\delta^{14}C/1000)) \cdot ((0.975)^2) \cdot ((1 + (\delta^{13}C/1000.)^{-2})] - 1.0\}$$

where $\delta^{14}C$ is defined as the relative difference between the absolute international standard activity (A_{abs}) and sample activity (A_s) that has been corrected for the age of the sample, but has not been corrected for $\delta^{13}C$:

$$\delta^{14}C = \{(A_S e^{\lambda(y-x)}/A_{abs}) - 1)\} \cdot 1000 \text{ per mil}$$

for the case of a tree ring grown in year x and measured in year y, and λ represents the 5730 year half-life of ^{14}C ($\lambda = 1/8267\,\text{yr}^{-1}$). Similarly:

$$\delta^{13}C = (R_S/R_{PDB} - 1) \cdot 1000$$

with R_S and R_{PDB} being the $^{13}C/^{12}C$ ratios of sample and a standard, respectively. The first of the above equations is commonly simplified to:

$$\Delta^{14}C = \delta^{14}C - 2 \cdot (\delta^{13}C + 25)(1 + (\delta^{14}C/1000.))$$

For the analysis considered here, the $\Delta^{14}C$ tracer is simplified by neglecting ^{13}C, although the tree-ring $\Delta^{14}C$ are normalized per convention. As long as one assumes that $\delta^{13}C$ is not affected by wind-driven changes in ocean dynamics and gas exchange, the

variability of atmospheric $\Delta^{14}C$ can be identified approximately with changes in the ^{14}C-to-^{12}C ratio in the model atmosphere.

The zero level for $\Delta^{14}C$ is chosen to correspond to the $\Delta^{14}C$ of the absolute radiocarbon standard, which is 1890 wood (Broecker and Olson, 1959). For the pre-anthropogenic climate system, one usually assumes a "mean state" with $\Delta^{14}C = 0‰$ in the atmosphere where decay is balanced by production of ^{14}C in the upper atmosphere through the effect of cosmic rays (spallation). It is thought that spallation produces equal amounts of ^{14}C in either hemisphere, with the transport of ^{14}C between the stratosphere and the troposphere occurring nearly completely in the hemisphere where ^{14}C was produced. The sum of the spallation-production in the atmosphere is balanced by the decay of ^{14}DIC in the ocean interior, and to a lesser degree in the atmosphere and the terrestrial biosphere, via radioactive decay. For this pre-anthropogenic state, scaling arguments indicate that the net radiocarbon fluxes into the terrestrial biosphere were relatively small, as described in Sect. 2b. The variations of $\Delta^{14}C$ shown in Fig. 1 are thought of as being small perturbations about this steady state.

The atmospheric $\Delta^{14}C$ values used in the study are taken from the IntCal04 (Reimer et al., 2004) and SHCal04 (McCormac et al., 2004) data sets. The IntCal04 data set is based on single year radiocarbon analyses of tree-rings from the US Pacific coast for the period AD 1510–1950 and 10-year blocks of tree-ring measurements for the entire period from both US and British Isle trees as described in Reimer et al. (2004). The data were combined using a random walk model (Buck et al., 2004) and evaluated at 5-year resolution. The SHCal04 dataset was similarly modeled from single or multiple blocks of tree-ring radiocarbon analyses from Chilean wood for the period AD 1665–1950 and 10-year blocks of tree-rings from New Zealand and South Africa (Hogg et al., 2002; McCormac et al., 2004).

Appendix B

Monte Carlo simulations for change point tests

In order to independently test the hypothesis that there is a shift in the interhemispheric gradient associated with the Medieval Climate Anomaly and the Little Ice Age, we apply the change point test developed by Worsley (1979) to the time series for $\Delta^{14}C$ in Fig. 1b over AD 950–1830. This approach allows one to test whether a shift in the mean occurs, and in the latter case to determine when it occurs. A significant shift in the mean (>99% confidence level) was detected in 1375, with the mean before the change being −6.63‰ and the mean after the change being −4.48‰. To verify that the variance remains constant in time, we applied the test for a shift in variance developed by Inclan and Tiao (1994) and found (at the 95% confidence level) that the variance does not seem to change over the interval 950–1830. The analysis was repeated for the time interval AD 950–1860 (instead of 950–1830) and the same transition in AD 1375 was identified. Thus this result is not sensitive to the whether one includes growth in $^{14}CO_2$-depleted fossil fuels over the period 1830–1860.

In the parlance of climate science, the time series contains red noise. Due to the presence of red noise in the time series, the confidence levels presented above were obtained through Monte Carlo simulations with a similar methodology as used by Wang (2008). Hence, the techniques developed by Worsley (1979) and Inclan and Tiao (1994) were designed for independent (no correlation in time) and identically disributed normal errors. When these conditions do not apply, the distributions of the statistical tests of Worsley (1979) can be affected, and thus the percentiles derived under the assumption of independence and identically distributed normal errors are inappropriate. We were cautious about this point in the analysis presented here. For this reason, we used Monte Carlo simulations to obtain the critical values of these two statistics under a red noise model. We consider the red noise model in the residuals after subtracting the means to avoid a shift in the mean to interfere with the estimation of the parameters

of the model. We identified that the residuals can be represented by a second order autocorrelation model (AR(2)) which can be expressed as:

$$x_i = 1.02x_{i-1} - 0.25x_{i-2} + e_i$$

where x_i designates the $\Delta^{14}C$ at time t and e_i is the white noise residual. Using this model, we generated 10 000 time series of random numbers from a Normal distribution having the same red noise characteristics (length, white noise variance, and autocorrelation parameters) as observed in the $\Delta^{14}C$ residuals. These two change point statistics were computed in all synthetic series and the critical values of the two change point statistics were obtained. These new critical values were used to test for a shift in the mean and in the variance of Sect. 1, instead of the original critical values presented in Worsley (1979) and Inclan and Tiao (1994), which were obtained under the independence assumption.

Acknowledgements. This report was prepared by K. B. R. under awards NA17RJ2612 and NA08OAR4320752, which includes support through the NOAA Office of Oceanic and Atmospheric Research (OAR) through the Office of Climate Observations (OCO). We wish to thank DOE for their support through DE-FG02-07ER64467, NOAA for their CPT support through NOAA NA07OAR4310096, and both BP and the Ford Motor Company for support through the Carbon Mitigation Initiative (CMI) at Princeton University. Support for S.E. Mikaloff Fletcher comes from the New Zealand Research Foundation for Research, Science and Technology, contract number C01X0703, as well as ESRL funding through NOAA/CICS award NA08OAR4320752. Support for C. B. came through Fonds Québécois de la Recherche sur la Nature et les technologies in addition to the CMI.

References

Aumont, O.: Étude du cycle naturel du carbone dans un modèle 3-D de l'océan mondial, PhD. Thesis, Univ. Paris VI, Paris, 1998.

Böning, C., Dispert, A., Visbeck, M., Rintoul, S., and Scharzkopf, F.: The response of the Antarctic Circumpolar Current to recent climate change, Nat. Geosci., 1, 864–869, 2008.

Braziunas, T. F., Fung, I. Y., and Stuiver, M.: The preindustrial atmospheric $^{14}CO_2$ latitudinal gradient as related to exchanges among atmospheric, oceanic, and terrestrial reservoirs, Global Biogeochem. Cy., 9(4), 565–584, 1995.

Broecker, W. S. and Olson, E. A.: Lamont Radiocarbon Measurements VI, Radiocarbon, 1(1), 111–132, 1959.

Buck, E. and Blackwell, P. G.: Formal statistical models for estimating radiocarbon calibration curves, Radiocarbon, 46(3), 1093–1102, 2004.

Cobb, K. M., Charles, C. D., Edwards, R. L., Cheng, H., and Kastner, M.: El Niño-Southern Oscillation and tropical Pacific climate during the last millennium, Nature, 242, 271–276, 2003.

da Silva, A., Young, A. C., and Levitus, S.: Atlas of Surface marine Data 1994, Vol. 1, Algorithms and Procedures, NOAA Atlas NESDIS 6, Natl. Oceanic and Atmos. Admin., Silver Spring, Md, 1994.

d'Orgeville, M., Sijp, W. P., England, M. H., and Meissner, K. J.: On the control of glacial-interglacial atmospheric CO_2 variations by the Southern Hemisphere westerlies, Geophys. Res. Lett., 37, L21703, doi:10.1029/2010GL045261, 2010.

Farneti, R., Delworth, T. I., Rosati, A. J., Griffies, S. M., and Zhang, F.: The role of mesoscale eddies in the rectification of the Southern Ocean response to climate change, J. Phys. Oceaonogr., 40, 7, 1539–1557, 2010.

Galbraith, E. D., Kwon, E. Y., Gnanadesikan, A., Rodgers, K. B., Griffies, S. M., Bianchi, D., Sarmiento, J. L., Dunne, J. P., Simeon, J., Slater, R. D., Wittenberg, A. T., and Held, I. M.: The Impact of Climate Variability on the Distribution of Radiocarbon in CM2Mc, a New Earth System Model, J. Climate, accepted, 2011.

Geller, L. S., Elkins, J. W., Lobert, J. M., Clarke, A. D., Hurst, D. F., Butler, J. H., and Myers, R. C.: Tropospheric SF_6: Observed latitudinal distribution and trends, derived emissions and interhemispheric exchange time, Geophys. Res. Lett., 24(6), 675–678, 1997.

Gnanadesikan, A., Slater, R. D., Gruber, N., and Sarmiento, J. L.: Ocean vertical exchange

and new production: a comparison between models and observations, Deep-Sea Research II 49, 363–401, 2002.
Gnanadesikan, A., Dunne, J. P., Key, R. M., Matsumoto, K., Sarmiento, J. L., Slater, R. D., and Swathi, P. S.: Ocean ventilation and biogeochemical cycling: Understanding the physical mechanisms that produce realistic distributions of tracers and productivity, Global Biogeochem. Cy., 18, BG4010, doi:10.1029/2003GB002087, 2004.
Hallberg, R. and Gnanadesikan, A.: The role of eddies in determining the structure and response of the wind-drive Southern Hemisphere overturning: Results from the Modeling Eddies in the Southern Ocean (MESO) project, J. Phys. Oceanogr., 36, 2232–2252, 2006.
Heimann, M. and Körner, S.: The global atmospheric tracer model TM3, in Max-Planck-Institut für Biogeochemie (Eds.): Technical Resport, Vol. 5, Max-Planck-Institut für Biogeochemie, Jena, 131 Pp., [BGC0601; ECO140/036+5], 2003.
Hogg, A. G., McCormac, F. G., Higham, T. F. G., Reimer, P. J., Baillie, M. G. L., and Palmer, J. G.: High-precision radiocarbon measurements of contemporaneous tree-ring dated wood from the British Isles and New Zealand: AD 1850–950, Radiocarbon, 44(3), 633–650, 2002.
Inclan, C. and Tiao, G.: Use of cumulative sums of squares for retrospective detection of changes in variance, J. Am. Stat. Assoc., 89, 913–923, 1994.
Jungclaus, J. H., Lorenz, S. J., Timmreck, C., Reick, C. H., Brovkin, V., Six, K., Segschneider, J., Giorgetta, M. A., Crowley, T. J., Pongratz, J., Krivova, N. A., Vieira, L. E., Solanki, S. K., Klocke, D., Botzet, M., Esch, M., Gayler, V., Haak, H., Raddatz, T. J., Roeckner, E., Schnur, R., Widmann, H., Claussen, M., Stevens, B., and Marotzke, J.: Climate and carbon-cycle variability over the last millennium, Clim. Past, 6, 723–737, doi:10.5194/cp-6-723-2010, 2010.
Kalnay, E. C., Kanamitsu, M., Kistler, R., Collins, W., Deaven, D., Gandin, L., Iredell, M., Saha, S., White, G., Woollen, J., Zhu, Y., Chellian, M., Ebisuzaki, W., Higgins, W., Janowiak, J., Mo, K. C., Ropelewski, C., Wang, J., Leetmaa, A., Reynolds, R., Jenne, R., and Joseph, D.: The NCEP/NCAR reanalysis project, Bull. Am. Meteor. Soc., 77, 347–471, 1996.
Key, R. M., Kozyr, A., Sabine, C. L., Lee, K., Wanninkhof, R., Bullister, J. L., Feely, R. A., Millero, F. J., Mordy, C., and Peng, T.-H.: A global ocean carbon climatology: Results from Global Data Analysis Project (GLODAP), Global Biogeochem. Cy., 18, BG4031, doi:10.1029/2004GB002247, 2004.
Krakauer, N. Y., Randerson, J. T., Primeau, F. W., Gruber, N., and Menemenlis, D.: Carbon isotope evidence for the latitudinal distribution and wind speed dependence of the air-sea

gas transfer velocity, Tellus 58B, 390–417, 2006.
Le Quéré, C., Rödenbeck, C., Buitenhuis, E. T., Conway, T. J., Langenfelds, R., Gomez, A., Labuschagne, C., Ramonet, M., Nakazawa, T., Metzl, N., Gillett, N., and Heimann, M.: Saturation of the Southern Ocean CO_2 sink due to recent climate change, Science, 316(5832), 1735–1738, 2007.
Levin, I. and Hesshaimer, V.: Radiocarbon – A Unique Tracer of Global Carbon Cycle Dynamics, Radiocarbon, 42, 69–80, 2000.
Levin, I., Naegler, T., Kromer, B., Diehl, M., Francey, R. J., Gomez-Pelaez, A. J., Steele, L. P., Wagenbach, D., Weller, R., and Worthy, D. E.: Observations and modelling of the global distribution and long-term trend of atmospheric $^{14}CO_2$, Tellus B, 62(1), 26–46, 2009.
Lintner, B. R., Gilliland, A. B., and Fung, I. Y.: Mechanisms of convection-induced modulation of passive tracer interhemispheric transport interannual variability, J. Geophys. Res.-Atmos., 109(D13), doi:10.1029/2003JD004306, 2004.
Lund, D. C., Lynch-Stieglitz, J., and Curry, W. B.: Gulf stream density structure and transport during the past millennium, Nature, 444, 601–604, 2006.
Marchal, O., Stocker, T. F., and Muscheler, R.: Atmospheric radiocarbon during the Younger Dryas: production, ventilation, or both?, Earth Planet. Sc. Lett., 185, 383–395, 2001.
Masarik, J. and Beer, J.: Simulation of particle fluxes and cosmogenic radionuclide formation in Earth's atmosphere, J. Geophys. Res., 104(D10), 12099–13012, 1999.
McCormac, F. G. Reimer, P. J., Hogg, A. G., Higham, T. F. G., Baillie, M. G. L., Palmer, J., and Stuiver, M.: Calibration of the radiocarbon time scale for the Southern Hemisphere: AD 1850–950, Radiocarbon, 44(3), 641–651, 2002.
McCormac, F. G., Hogg, A. G., Blackwell, P. G., Buck, C. E., Higham, T. F. G., and Reimer, P. J.: SHCAL04 Southern Hemisphere Calibration, 0–11 cal kyr BP, Radiocarbon, 46(3), 1087–1092, 2004.
Meissner, K. J., Younger Dryas: A data to model comparison to constrain the strength of the overturning circulation, Geophys. Res. Lett., 34, L21705, doi:10.1029/2007GL031304, 2007.
Mignone, B. K., Gnanadesikan, A., Sarmiento, J. L., and Slater, R. D.: Central Role of Southern Hemisphere winds and eddies in modulating the oceanic uptake of anthropogenic carbon, Geophys. Res. Lett., 33, L01604, doi:10.1029/2005GL024464, 2006.
Naegler, T., Ciais, P., Rodgers, K., and Levin, I.: Excess radiocarbon constraints on air-sea gas exchange and the uptake of CO_2 by the oceans. Geophys. Res. Lett., 33, L11802,

doi:10.1029/2005GL025408, 2006.
Naegler, T.: Reconciliation of excess ^{14}C-based global CO_2 piston velocity estimates, Tellus 61B, 372–384, doi:10.1111/j.1600-0889.2008.00408.x, 2009.
Pacanowski, R. C. and Griffies, S. M.: The MOM3 manual, alpha version, NOAA/Geophys. Fluid Dyn. Lab., Princeton, N.J., 1999.
Randerson, J. T., Thompson, M. V., Conway, T. J., Fung, I. Y., and Field, C. B.: The contribution of terrestrial sources and sinks to trends in the seasonal cycle of atmospheric carbon dioxide, Global Biogeochem. Cy., 11(4), 535–560, 1997.
Randerson, J. T., Enting, I. G., Schnurl, A. A. G., Caldeira, K., and Fung, I. Y.: Seasonal and latituindal variability of troposphere $\Delta^{14}CO_2$: Post bomb contributions from fossil fuels, oceans, the stratosphere, and the terrestrial biosophere, Global Biogeochem. Cy., 16(4), 1112, doi:10.1029/2002GB001876, 2002.
Reimer, P. J., Baillie, M. G. L., Bard, E., Bayliss, A., Beck, J. W., Bertrand, C. J. H., Blackwell, P. G., Buck, C. E., Burr, G. S., Cutler, K. B., Damon, P. E., Edwards, R. L., Fairbanks, R. G., Friedrich, M., Guilderson, T. P., Hott, A. G., Hughen, K. A., Kromer, B., McCormac, G., Manning, S., Ramsey, C. B., Reimer, R. W., Remmele, S., Southon, S. R., Stuiver, M., Talamo, S., Taylor, F. W., van der Plicht, J., and Weyhenmeyer, C. E.: INTCAL Terrestrial Radiocarbon Age Calibration, 0–26, Cal kyr AP, Radiocarbon, 46(3), 1029–1058, 2004.
Rödenbeck, C., Le Quéré, C., Heimann, M., and Keeling, R. F.: Interannual variability in oceanic biogeochemical processes inferred by inversion of atmospheric O_2/N_2 and CO_2 data, Tellus, Ser. B., 60, 685–705, 2008.
Sachs, J. P., Sachse, D., Smittenberg, R. H., Zhang, Z., Battisti, D. S., and Golubic, S.: Southward movement of the Pacific intertropical convergence zone AD 1400–1850, Nature Geoscience, 2, 519–525, 2009.
Sigenthaler, U., Carbon Dioxide: Its natural cycle and anthropogenic perturbation, in: The role of air-sea gas exchange in geochemical cycling, edited by: Buat-Ménard, P., 209–247, D. Reidel, Dordecht, 1986.
Siegenthaler, U., Heimann, M., and Oeschger, H.: ^{14}C Variations caused by changes in the global carbon cycle, Radiocarbon, 22(2), 177–191, 1980.
Skinner, L. C., Fallon, S., Waelbroeck, C., Michel, E., and Barker, S.: Ventilation of the Deep Southern Ocean and Deglacial CO_2 Rise, Science, V. 328, 1147–1151, 2010.
Straub, D. N.: On the transport and angular momentum balance of channel models of the Antarctic Circumpolar Current, J. Phys. Oceanogr., 23, 776–782, 1993.

Stuiver, M., and H.A. Polach, Discussion reporting of ^{14}C data, Radioarbon, Vol. 19, No. 3, 355-363, 1977.
Stuiver, M. and Quay, P. D.: Changes in Atmospheric Carbon-14 attributed to a variable sun, Science, 207, 4426, 11–19, 1980.
Sweeney, C., Gloor, E., Jacobson, A. R., Key, R. M., McKinlye, G., Sarmiento, J. L., and Wanninkhof, R.: Constraining air-sea gas exchange for CO_2 with recent bomb ^{14}C measurements, Global Biogeochem. Cy., 21, GB2015, doi:10.1029/2006GB002784, 2007.
Toggweiler, J. R., and Samuels, B.L Is the magnitude of the deep outflow from the Atlantic Ocean actually governed by Southern Hemisphere winds, NATO ASI Series, Vol. 115, The Global Carbon cycle, edited by: Martin Heimann, 1993.
Trenberth, K. E., Olsen, J. G., and Large, W. G.: A global ocean wind stress climatology based on ECMWF analyses, Tech Rep. NCAR/TN-335+STR, Natl. Cent. For Atmos. Res., Boulder, Colo., 1989.
Turnbull, J. C., Miller, J. B., Lehman, S. J., Hurst, D., Peters, W., Tans, P. P., Southon, J., Montzka, S. A., Elkins, J. W., Mondeel, D. J., Romashkin, P. A., Elansky, N., and Skorokhod, A.: Spatial distribution of $\Delta^{14}CO_2$ across Eurasia: measurements from the TROICA-8 expedition, Atmos. Chem. Phys., 9, 175–187, doi:10.5194/acp-9-175-2009, 2009.
Turney, C. S. M., and Palmer, J.: Does the El Nino-Southern Oscillation control the interhemispheric radiocarbon offset? Quaternary Res., 67, 174–180, 2007.
Wang, X. L.: Accounting for autocorrelation in detecting mean shifts in climate data series, using the penalized maximum t or F test, J. Appl. Meteorol. Clim., 47, 2423–2444, 2008.
Wanninkhof, R.: Relationship between gas exchange and wind speed over the ocean, J. Geophys. Res., 97, 7373–7381, 1992.
Wanninkhof, R. and McGillis, W. R.: A cubic relationship between air-sea CO_2 exchange and windspeed, Geophys. Res. Lett., 26(13), 1889–1892, 1999.
Worsley, K. J.: On the likelihood ratio test for a shift in location of normal populations, Journal of the American Statistical Association, 74, 365–367, 1979.
Visbeck, M.: A station-based Southern Annular Mode Index from 1884 to 2005, J. Climate, 22, 940–950, 2009.

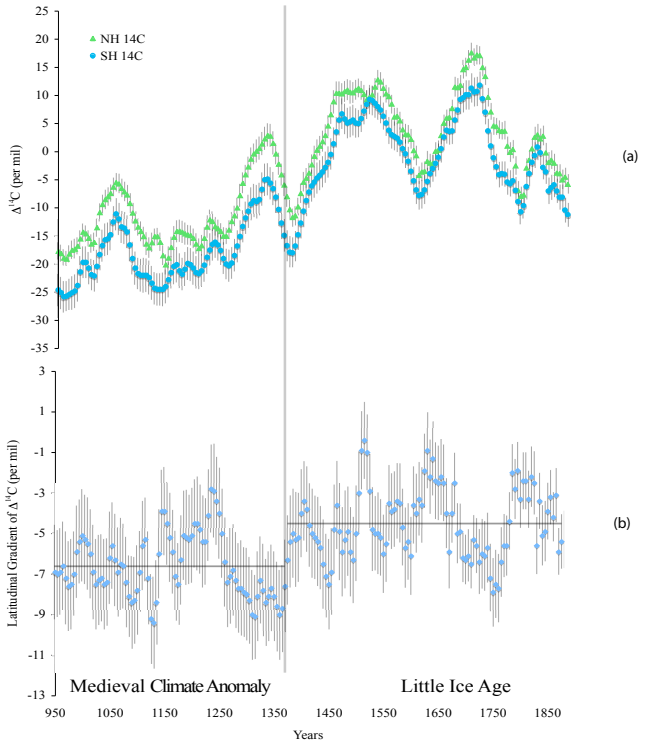

Fig. 1. Tree ring proxy records of atmospheric $\Delta^{14}C$ over the period 950–1830; **(a)** The Northern Hemispehre INTCAL04 record (Reimer et al., 2004) is shown as triangles, the Southern Hemisphere SHCAL04 (McCormac et al., 2004) record as circles. The temporal resolution of each record is five years. **(b)** The Interhemispheric Gradient in atmospheric $\Delta^{14}C$, again with five-year resolution.

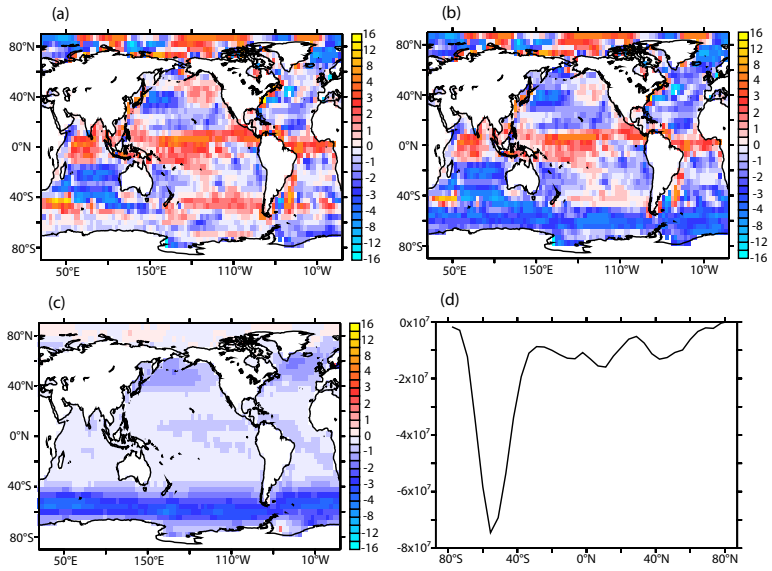

Fig. 2. Surface annual mean air-sea tracer fluxes from the mean state of the MOM3 ocean model. **(a)** CO_2 flux (mol C m^{-2} s^{-1}). **(b)** $^{14}CO_2$ flux (scaled via multiplication by the late 19th centry ratio of $^{12}CO_2/^{14}CO_2$, or $\Delta^{14}C = 0$, in the atmosphere) (mol C m^{-2} s^{-1}). **(c)** Disequilbrium Flux ϕ_{diseq} [$^{14}CO_2$ flux (scaled) minus CO_2 flux] (mol C m^{-2} s^{-1}). **(d)** Zonal integral of the Disequilbrium Flux ϕ_{diseq}.

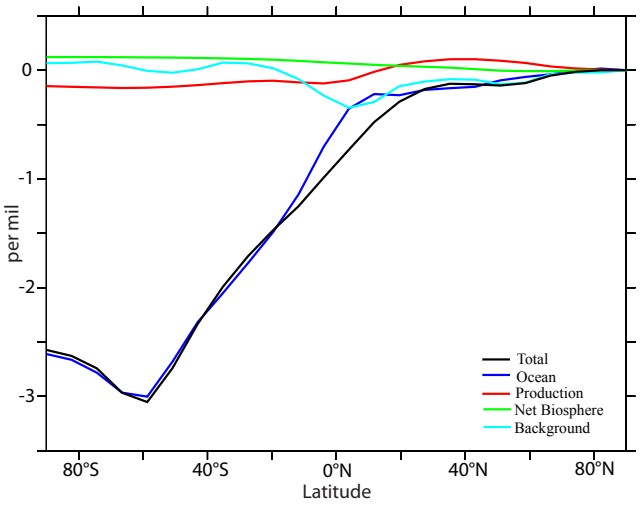

Fig. 3. The mean meridional structure of $\Delta^{14}C$ in the atmospheric boundary layer of the Atmospheric Transport Model under steady-state cyclostationary conditions, shown as deviations from the $\Delta^{14}C$ activity simulated at the North Pole. Shown are the total structure of the interhemispheric gradient (black), the component due to air-sea fluxes of CO_2 and $^{14}CO_2$ (blue), the component due to spallation/production of $^{14}CO_2$ in the atmosphere (red), and the component due to the net biosphere disequilibrium (green). (per mil).

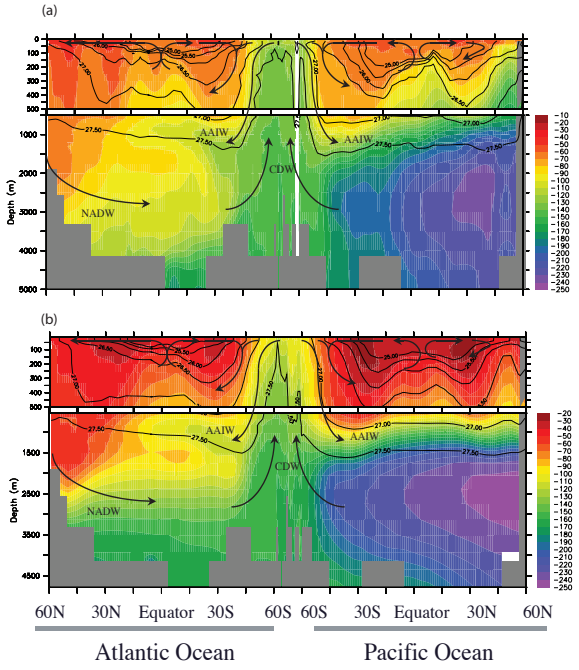

Fig. 4. Southern Ocean-centric view of pre-bomb $\Delta^{14}C$ in the ocean interior (per mil). **(a)** GLODAP (Key et al., 2004). **(b)** MOM3 P2A (Gnanadesikan et al., 2002; Gnanadesikan et al., 2004).

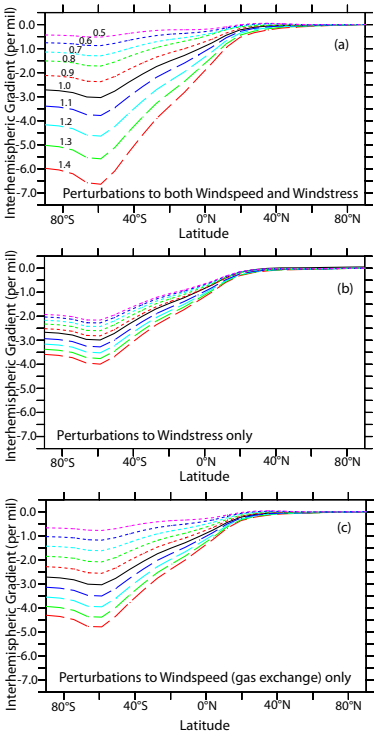

Fig. 5. Response of zonal surface $\Delta^{14}C$ to Southern Ocean wind perturbations (per mil deviations from value at North Pole for each case). **(a)** Perturbation applied to both wind stress (dynamical forcing) and wind speed (gas exchange). **(b)** Perturbation applied to gas exchange (but not wind stress). **(c)** Perturbation appied to wind stress (but not gas exchange).

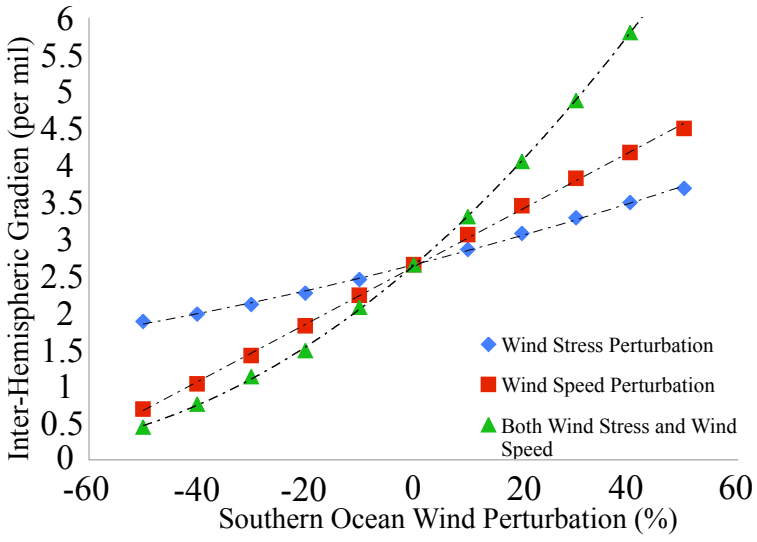

Fig. 6. Scatterplot of response of the Interhemispheric Gradient of atmospheric $\Delta^{14}C$ to surface windspeed perturbations after 20 years.

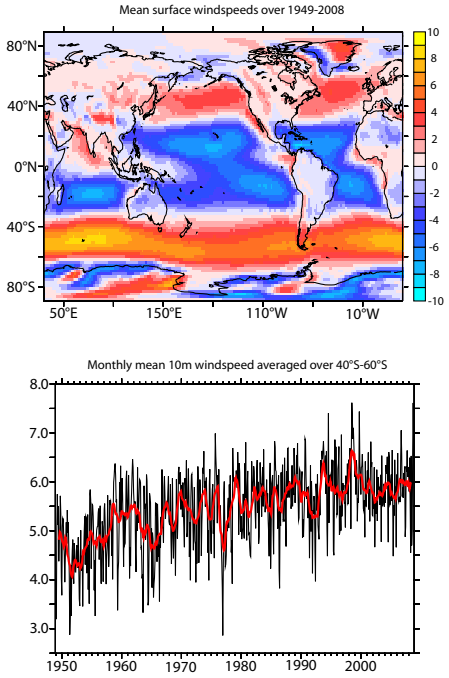

Fig. 7. NCEP (Kalnay et al., 1996) monthly mean 10 m windspeeds [m/s]. **(a)** Average over 1949–2008. **(b)** Timeseries over 1949–2008 of monthly mean values averaged over 40° S–60° S.